

# A Nickel-Manganese Catalyst as Biomimic of the active site of NiFe hydrogenases: a Combined Electrocatalytical and DFT Mechanistic Study

## Supplementary information

Vincent Fourmond, Sigolène Canaguier, Benjamin Golly,  
 Martin J. Field, Marc Fontecave and Vincent Artero

### 1 Supplementary DFT results

| Bond/Angle               | $1^+$        | [NiMn]       | [NiMn] <sup>-</sup> | [NiHMn]      | [Ni(H <sub>2</sub> )Mn] <sup>+</sup> | [NiMn] <sup>+</sup> | [NiHMn] <sup>-</sup> | [Ni(H <sub>2</sub> )Mn] |
|--------------------------|--------------|--------------|---------------------|--------------|--------------------------------------|---------------------|----------------------|-------------------------|
| Ni–Mn                    | 3.172        | 2.992        | 2.901               | 2.801        | 3.082                                | 2.954               | 2.670                | 2.933                   |
| Mn–OH <sub>2</sub>       | 2.193        |              |                     |              |                                      |                     |                      |                         |
| Mn–H                     |              |              |                     | 1.615        | 1.802, 1.812                         |                     | 1.638                | 1.773, 1.807            |
| Ni–H                     |              |              |                     | 2.067        | 2.365, 3.128                         |                     | 1.775                | 2.049, 2.854            |
| Ni–H–Mn                  |              |              |                     | 98.3         | 51.6, 42.8                           |                     | 102.9                | 97.8, 73.7              |
| Mn–CO <sub>average</sub> | 1.803, 1.790 | 1.782, 1.812 | 1.772, 1.799        | 1.777, 1.818 | 1.818, 1.825                         | 1.816, 1.793        | 1.772, 1.804         | 1.805, 1.814            |
| Ni–Mn–CO                 | 127.2, 115.6 | 114.5, 134.8 | 114.2, 134.6        | 117.2, 131.0 | 118.4, 134.4                         | 118.4, 134.2        | 114.9, 134.4         | 125.5, 118.0            |
| Hinge Ni-2S-Mn           | 122.3        | 114.2        | 108.5               | 101.6        | 115.9                                | 113.8               | 94.5                 | 108.3                   |
| Hinge 2S-Ni-2S           | 170.3        | 173.2        | 173.7               | 177.5        | 169.3                                | 172.8               | 174.3                | 168.8                   |

**Table S1:** DFT (B3LYP) in DMF optimized structural data for the species in the H<sub>2</sub>-evolving catalytic cycles of  $1^+$ .

| Atom | [NiMn] | [NiMn] <sup>-</sup> | [NiHMn] <sup>-</sup> | [Ni(H <sub>2</sub> )Mn] |
|------|--------|---------------------|----------------------|-------------------------|
| Mn   | 0.897  | 0.895               | -0.014               | -0.011                  |
| Ni   | 0.006  | -0.749              | 0.838                | 0.805                   |
| Sab  | 0.010  | -0.068              | 0.059                | 0.064                   |
| Scd  | 0.003  | -0.038              | 0.037                | 0.046                   |

**Table S2:** Mulliken spin densities for the intermediate species in the H<sub>2</sub>-evolving catalytic cycle of  $1^+$  (B3LYP in DMF). Only structures with non-zero spin densities are shown.

| Atom     | $1^+$         | [NiMn]         | [NiMn] <sup>-</sup> | [NiHMn]        | [Ni(H <sub>2</sub> )Mn] <sup>+</sup> | [NiMn] <sup>+</sup> | [NiHMn] <sup>-</sup> | [Ni(H <sub>2</sub> )Mn] |
|----------|---------------|----------------|---------------------|----------------|--------------------------------------|---------------------|----------------------|-------------------------|
| Mn       | 0.338         | -0.106         | 0.054               | 0.190          | 0.481                                | 0.367               | 0.630                | 0.322                   |
| Ni       | 0.380         | 0.386          | 0.392               | 0.282          | 0.357                                | 0.382               | 0.371                | 0.367                   |
| Water    | 0.101         |                |                     |                |                                      |                     |                      |                         |
| H        |               |                |                     | -0.313         | -0.184, 0.107                        |                     | -0.423               | -0.059, 0.068           |
| Total H  |               |                |                     |                | -0.077                               |                     |                      | 0.010                   |
| Sab      | -0.420        | -0.379         | -0.627              | -0.367         | -0.337                               | -0.353              | -0.638               | -0.559                  |
| Scd      | -0.121        | -0.207         | -0.311              | -0.089         | -0.155                               | -0.235              | -0.198               | -0.222                  |
| Total S  | -1.083        | -1.173         | -1.875              | -0.913         | -0.983                               | -1.176              | -1.671               | -1.562                  |
| CO       | -0.047, 0.003 | -0.195, -0.029 | -0.285, -0.078      | -0.125, -0.093 | -0.046, -0.055                       | -0.062, 0.028       | -0.253, -0.215       | -0.098, 0.018           |
| Total CO | -0.091        | -0.419         | -0.647              | -0.343         | -0.148                               | -0.096              | -0.721               | -0.178                  |

**Table S3:** Atomic (ESP) charges for the intermediate species in the H<sub>2</sub>-evolving catalytic cycle of  $1^+$  (B3LYP in DMF)

| Atom               | $1^+$        | [NiMn]       | [NiMn] <sup>-</sup> | [NiHMn]      | [Ni(H <sub>2</sub> )Mn] <sup>+</sup> | [NiMn] <sup>+</sup> | [NiHMn] <sup>-</sup> | [Ni(H <sub>2</sub> )Mn] |
|--------------------|--------------|--------------|---------------------|--------------|--------------------------------------|---------------------|----------------------|-------------------------|
| Ni–Mn              | 0.083        | 0.117        | 0.121               | 0.265        | 0.160                                | 0.142               | 0.297                | 0.174                   |
| Mn–OH <sub>2</sub> | 0.155        |              |                     |              |                                      |                     |                      |                         |
| Mn–H               |              |              |                     | 0.566        | 0.011, 0.012                         |                     | 0.498                | 0.254, 0.275            |
| Ni–H               |              |              |                     | 0.230        | 0.004, 0.000                         |                     | 0.356                | 0.105, 0.043            |
| H–H                |              |              |                     |              | 0.981                                |                     |                      | 0.580                   |
| Mn–Sab             | 0.687        | 0.622        | 0.624               | 0.588        | 0.748                                | 0.724               | 0.628                | 0.687                   |
| Ni–Sab             | 1.079        | 1.080        | 0.730               | 1.055        | 1.056                                | 1.084               | 0.647                | 0.720                   |
| Ni–Scd             | 0.918        | 0.850        | 0.625               | 0.838        | 0.882                                | 0.878               | 0.621                | 0.637                   |
| Mn–C               | 1.108, 1.159 | 1.242, 1.139 | 1.296, 1.188        | 1.214, 1.220 | 1.069, 1.150                         | 1.073, 1.143        | 1.235, 1.164         | 1.115, 1.065            |
| C–O                | 2.545, 2.532 | 2.347, 2.407 | 2.276, 2.316        | 2.373, 2.427 | 2.556, 2.540                         | 2.565, 2.551        | 2.355, 2.367         | 2.475, 2.560            |

**Table S4:** Mayer bond orders for the intermediate species in the H<sub>2</sub>-evolving catalytic cycle of  $1^+$  (B3LYP in DMF)

## 2 Supplementary electrochemical data

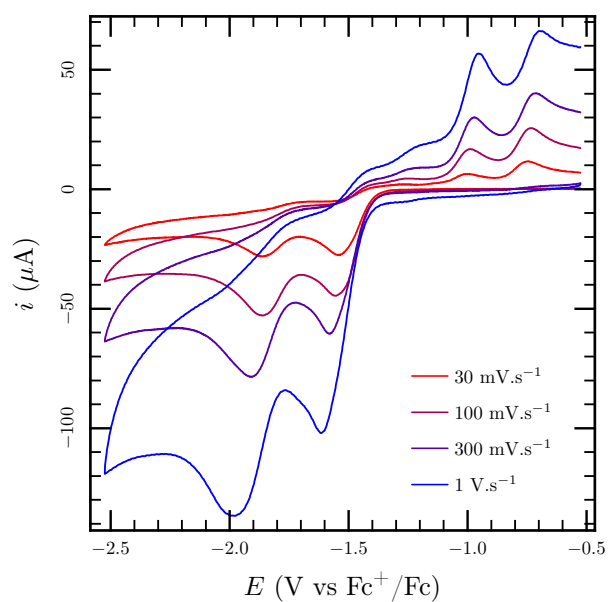


**Figure S1:** Voltammograms of 5 mmol.L<sup>-1</sup> of  $1Br$  in DMF with 0.1 mol.L<sup>-1</sup>  $nBu_4NBF_4$  as supporting electrolyte, in the absence of acid at various scan rates.

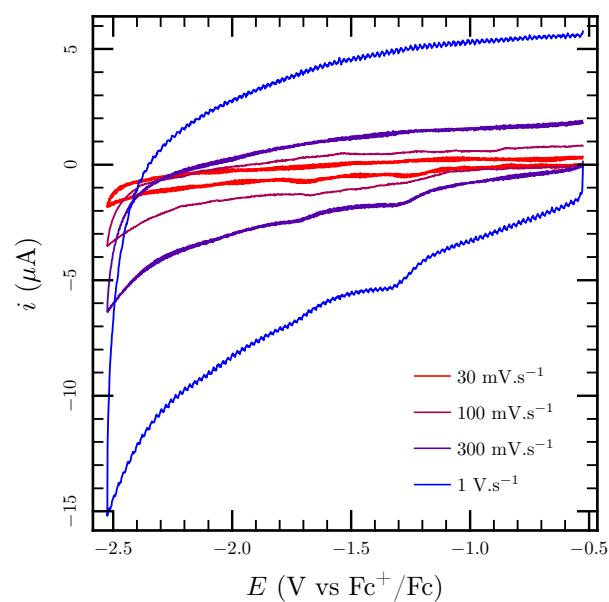


**Figure S2:** Blank voltammograms recorded at various scan rates in the same electrolyte as for figure S1, in the absence of any electroactive compound.

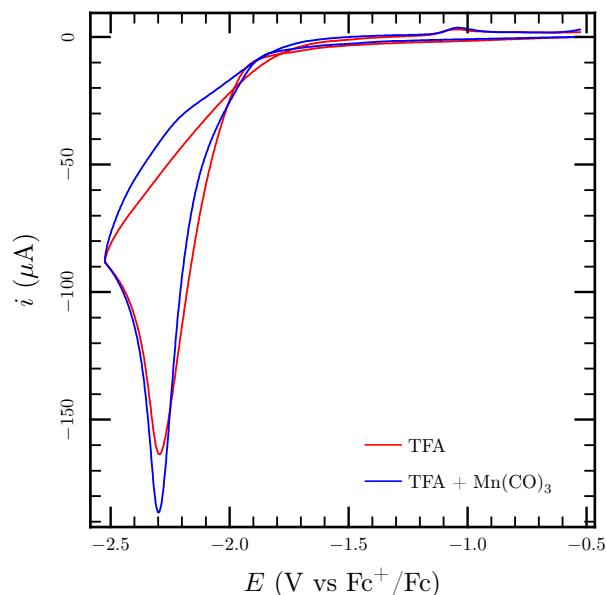


**Figure S3:** Cyclic voltammograms at a glassy carbon electrode in DMF ( $0.1 \text{ mol.L}^{-1} n\text{Bu}_4\text{NBF}_4$ ), in the presence of  $12 \text{ mmol.L}^{-1}$  TFA and in the absence (red line) or presence (blue line) of  $2 \text{ mmol.L}^{-1} [\text{Mn}(\text{CO})_3(\text{acetone})_3]^+$ . Scan rate:  $100 \text{ mV.s}^{-1}$ .

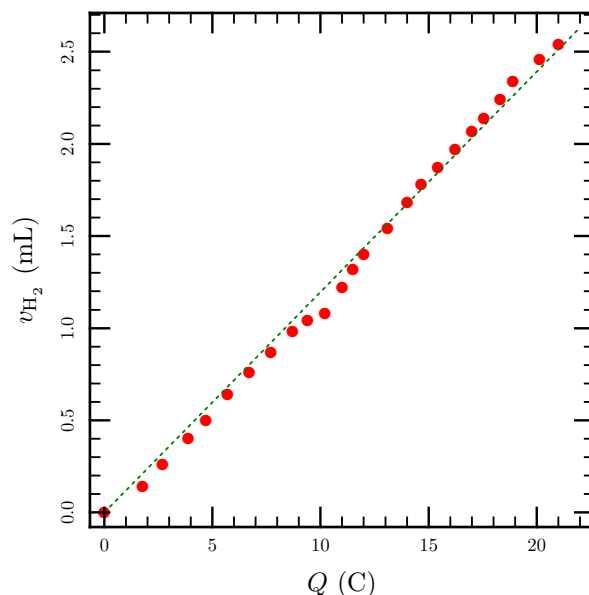


**Figure S4:** Volume of evolved  $\text{H}_2$  as a function of the total charge flowing through the electrode during a 4-hour electrolysis experiment at  $-1.82 \text{ V vs Fc}^+/\text{Fc}$  at a mercury pool electrode (area  $\approx 1.2 \text{ cm}^2$ ) of a  $7 \text{ mL}$  DMF solution containing  $0.1 \text{ mol.L}^{-1}$  TFA,  $1 \text{ mmol.L}^{-1}$   $1\text{Br}$  and  $0.1 \text{ mol.L}^{-1}$   $\text{Bu}_4\text{NBF}_4$  as supporting electrolyte. The dotted line corresponds to a linear slope of  $0.12 \text{ mL}(\text{H}_2.\text{C}^{-1})$ , i.e. a faradaic efficiency of 93% (conditions: atmospheric pressure and  $T = 298 \text{ K}$ ).

### 3 Properties of trifluoroacetic acid

We determined the  $\text{pK}_a$  of TFA in DMF using the fact that it is reduced reversibly at a platinum electrode (figure S5). Figure S6 show the half-sum of the reductive and oxidative peaks of the reduction of TFA at a platinum electrode in DMF; this data was fitted to the following equation, taken from reference 1<sup>1</sup>:

$$E_{1/2} = E_{\text{H}^+/\text{H}_2}^\circ - \frac{2.303 \times RT}{F} \text{pK}_a + \epsilon_D - \frac{RT}{2F} \ln \frac{C_0}{C_{\text{H}_2}^\circ} \quad (1)$$

where  $E_{\text{H}^+/\text{H}_2}^\circ = -0.62 \text{ V}$  is the standard potential for the reduction of protons in DMF,  $\epsilon_D = 40 \text{ mV}$  is a small correction factor,  $C_0$  is the total concentration of acid and  $C_{\text{H}_2}^\circ = 1.9 \text{ mmol.L}^{-1}$  the saturating concentration of dissolved  $\text{H}_2$  under 1 bar  $\text{H}_2$ . The fit is shown on figure S6 as green dotted lines; it gives  $\text{pK}_a = 6 \pm 0.3$ , which is reasonably close to the value extrapolated from a  $\text{pK}_a$  of 3.45 in DMSO [2] using the correlation described by Vianello and colleagues [3]:  $\text{pK}_{a\text{extrapolated}} = 4.9$ .

To obtain the diffusion coefficient, we have plotted (figure S7) the amplitude of the first reduction wave as a function of TFA concentration and plotted the values of slopes as a function of  $\sqrt{vF/RT}$ . For a purely diffusive reversible system, this is expected to give a linear dependency. For a simple one-electron electrode reaction, the relation between the slope of this line and the diffusion coefficient is given by [4]:

$$\alpha = F \times A \times \sqrt{D} \times 0.4463 \quad (2)$$

However, this equation does not apply here, as the reaction order at the electrode is not unity. As demonstrated by Shuman [5], a similar relation is expected to hold, but with a different numerical factor. We have performed simulations in the case of the acid reduction (figure S8), that show that the equation should read:

$$\alpha = F \times A \times \sqrt{D} \times 0.4107 \quad (3)$$

where  $F = 96485 \text{ C.mol}^{-1}$  is the Faraday constant,  $A = 3.14 \text{ mm}^2$  is the area of the electrode and  $D$  the diffusion coefficient, hence:

$$D = \left( \frac{\alpha}{0.4107 \times A \times F} \right)^2 \quad (4)$$

<sup>1</sup>See supplementary information of that publication for the reason why the half-sum of the reduction and oxidation potentials is likened to the half-wave potential.

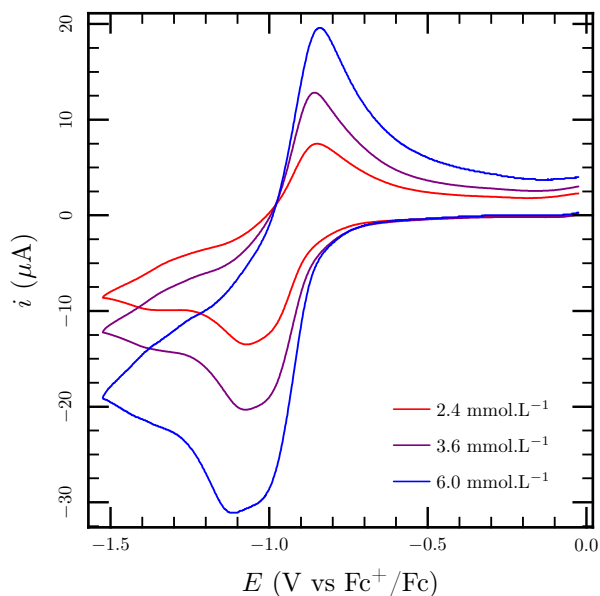


**Figure S5:** Voltammograms of various concentrations of TFA in DMF using 0.1 mol.L<sup>-1</sup>  $n\text{Bu}_4\text{NBF}_4$  as supporting electrolyte at a platinum electrode (2 mm diameter), showing that TFA is reduced reversibly at this electrode.

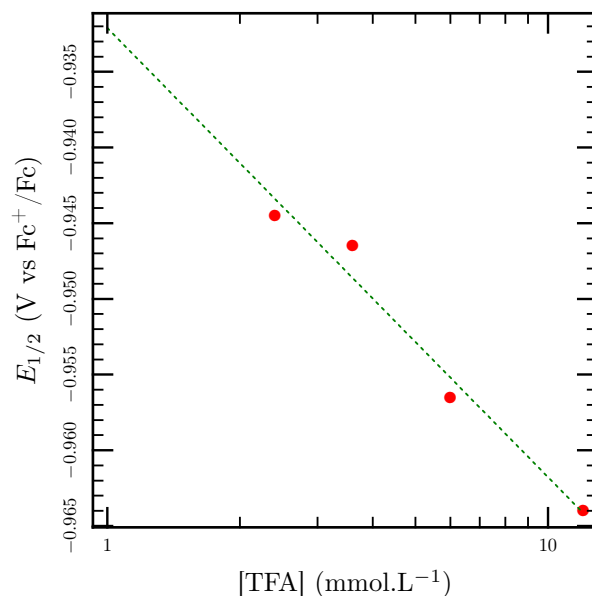


**Figure S6:** Half-sum of the reductive and oxidative peaks for the reversible reduction of TFA at a platinum electrode in DMF.

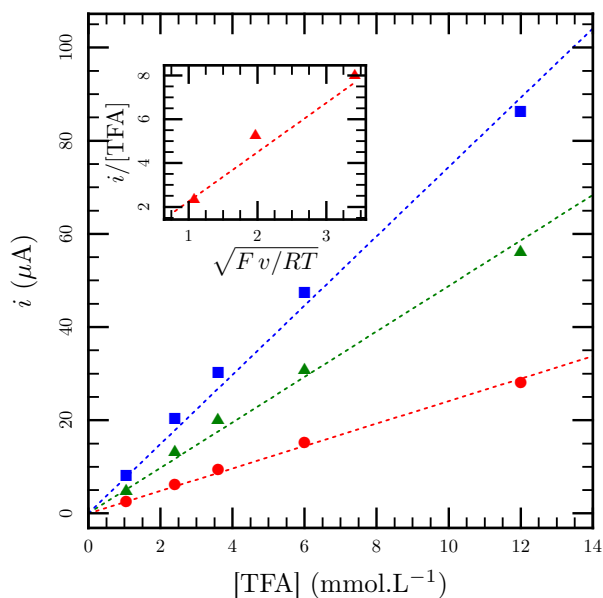


**Figure S7:** Reduction peak height for different scan rates (from bottom to top: 30 mV.s<sup>-1</sup>, 100 mV.s<sup>-1</sup> and 300 mV.s<sup>-1</sup>) as a function of TFA concentration, along with linear fits. Inset: a plot of the slopes found thus as a function of  $\sqrt{vF/RT}$ , along with a linear fit.

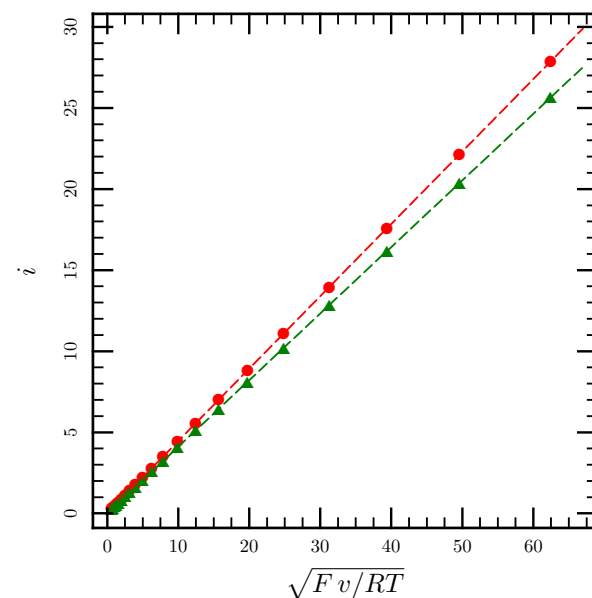


**Figure S8:** Plots of the peak intensity as a function  $\sqrt{Fv/RT}$  for two different systems: in red, a standard Ox + e<sup>-</sup> ⇌ Red electrode reaction and in green the 2AH + 2e<sup>-</sup> ⇌ 2A<sup>-</sup> + H<sub>2</sub> electrode reaction for acid reduction. Simulations were run with concentration and diffusion coefficients of 1, which means that the value of the slope equals the adimensional current  $\sqrt{\pi}\chi(at)$  defined in references 4 and 5. We found 0.4463 for the usual case, and 0.4107 for the acid reduction.

Converting  $\alpha$  to  $\text{A}\cdot\text{mol}^{-1}\cdot\text{cm}^3\cdot\text{s}^{1/2}$  and  $A$  in  $\text{cm}^2$  allows to obtain the diffusion coefficient in  $\text{cm}^2\cdot\text{s}^{-1}$ . Using a value of  $\alpha = 2.3 \pm 0.2$  gives  $D = 3.4 \pm 0.4 \times 10^{-6} \text{ cm}^2\cdot\text{s}^{-1}$ .

## 4 Does the protonation competes with or follows the post-reduction reorganisation ?

On of the mechanistic questions that one can ask oneself is whether the protonation follows the structural rearrangement that gives rise to the irreversibility of the second wave or if it competes with it. To discriminate between both possibilities, we have run simulations for both cases, and measured the position of the inflexion point of the catalytic wave as a function of the concentration of acid. Results of the simulations are shown on figure S9, while experimentally measured points are on figure S10. For experimental points, the inflexion point for the catalytic wave is shifted towards lower potentials when the  $\beta$  ratio increases. For simulated values, the inflexion point increases for the case when protonation competes with the structural rearrangement following the reduction, while it decreases in the case when protonation is following that structural rearrangement. This implies that most probably the protonation of  $[\text{NiMn}]^-$  is following the structural rearrangement following its reduction from  $[\text{NiMn}]$ , which is consistent with the expectation that a structural rearrangement will be fast enough to outcompete any bimolecular reaction.

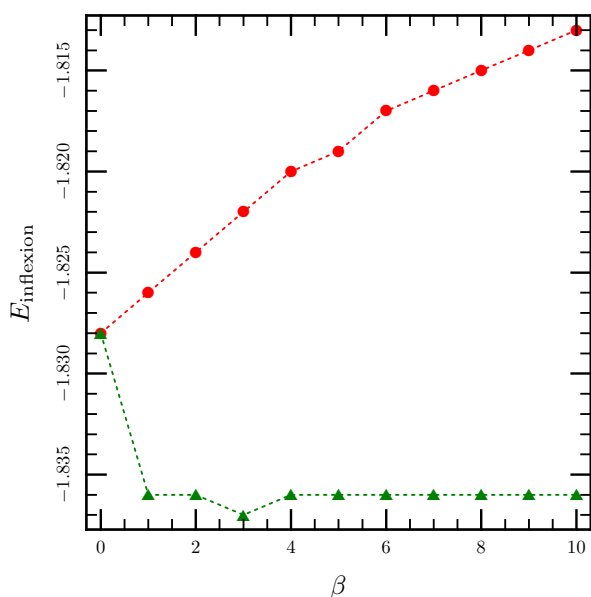


**Figure S9:** Position of the inflexion point of the catalytic wave as a function of  $\beta = [\text{AH}]/[\text{C}]$  (as in text) for different catalytic mechanisms differing only in the order of the protonation: red symbols are for the case when the protonation competes with the follow-up reaction while the green symbols are for the case when the protonation follows the structural rearrangement following the reaction.

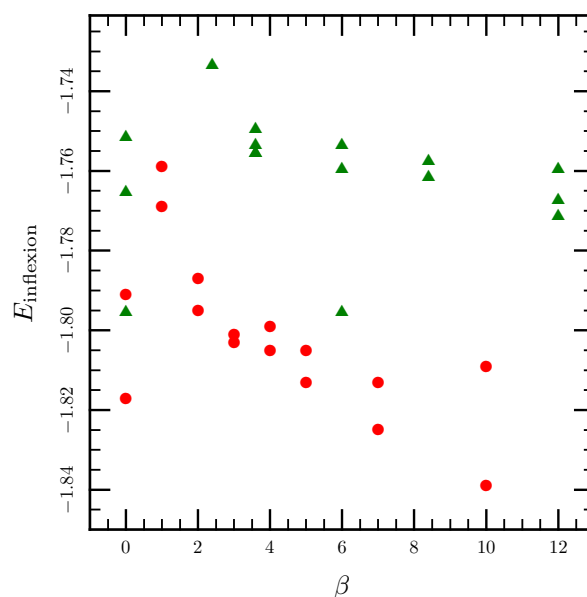


**Figure S10:** Position of the inflexion point of the catalytic wave measured for  $1 \text{ mmol}\cdot\text{L}^{-1}$  (green symbols) and  $5 \text{ mmol}\cdot\text{L}^{-1}$  (red symbols) as a function of  $\beta$  for a scan rate of  $100 \text{ mV}/\text{s}$ .

## 5 Simulations with other different ratios $k_{p1}/k_{p2}$

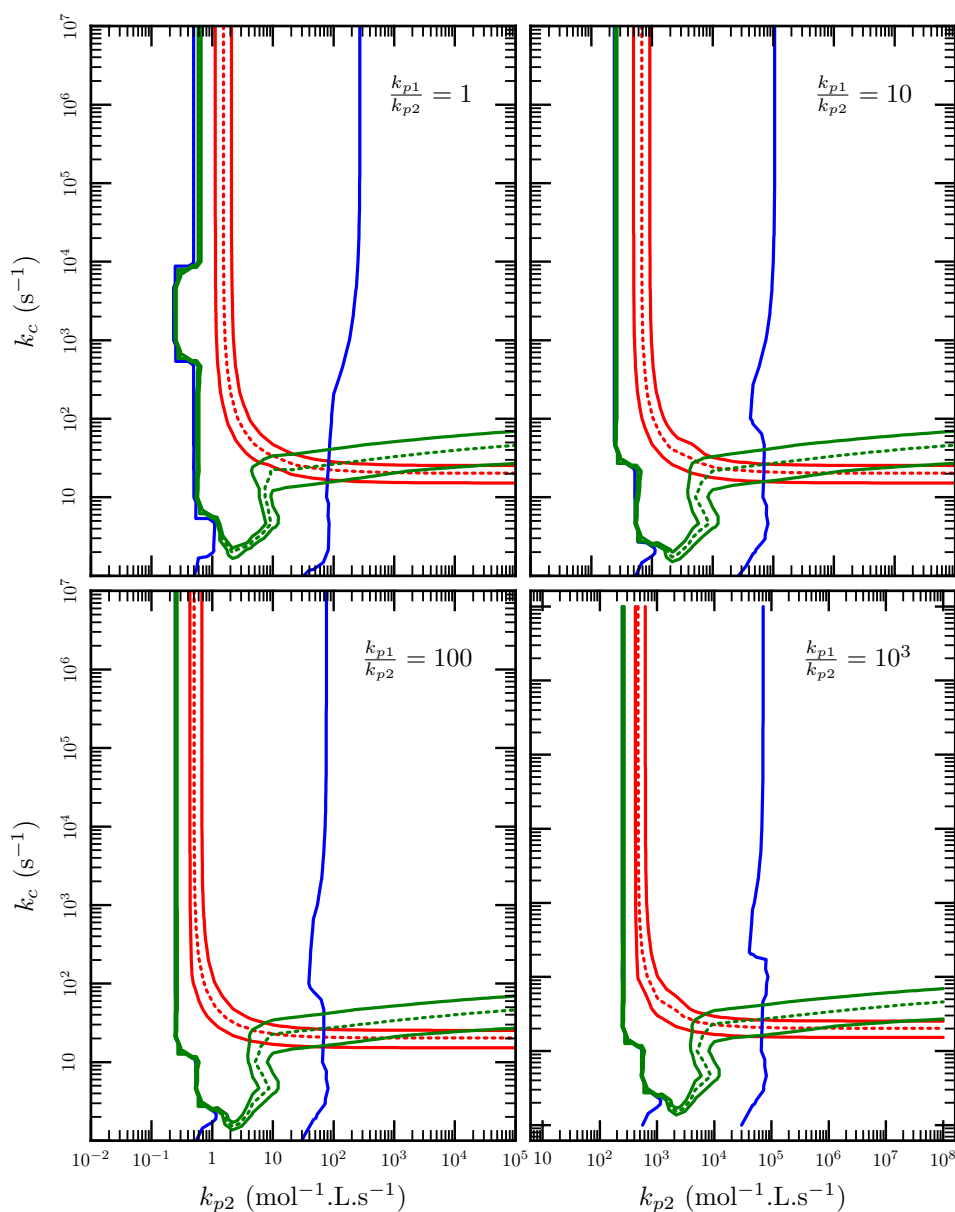


**Figure S11:** Pendants of the text figure 10D for values of the ratio  $k_{p1}/k_{p2}$  ranging from 1 to 1000, as indicated on each plot. As can be seen, changing this ratio hardly affects the results.

## References

- [1] V. Fourmond, P.-A. Jacques, M. Fontecave, and V. Artero.  $H_2$  evolution and molecular electrocatalysts: Determination of overpotentials and effect of homoconjugation. *Inorg. Chem.*, **49**, 10338–10347, 2010. doi: [10.1021/ic101187v](https://doi.org/10.1021/ic101187v).
- [2] K. Izutsu. *Acid-Base Dissociation Constants in dipolar aprotic solvents*. Number 35 in Chemical Data Series. Blackwell Scientific Publications, 1990.
- [3] F. Maran, D. Celadon, M. G. Severin, and E. Vianello. Electrochemical determination of the pKa of weak acids in N,N-dimethylformamide. *J. Am. Chem. Soc.*, **113**, 9320–9329, 1991. doi: [10.1021/ja00024a041](https://doi.org/10.1021/ja00024a041).
- [4] R. S. Nicholson and I. Shain. Theory of stationary electrode polarography. Single scan and cyclic methods applied to reversible, irreversible, and kinetic systems. *Anal. Chem.*, **36** (4), 706–723, 1964. doi: [10.1021/ac60210a007](https://doi.org/10.1021/ac60210a007).
- [5] M. S. Shuman. Nonunity electrode reaction orders and stationary electrode polarography. *Anal. Chem.*, **41**, 142–146, 1969. doi: [10.1021/ac60270a014](https://doi.org/10.1021/ac60270a014).